Available online at www.sciencedirect.com
SCIENCE DIRECT®
International Journal of Mass Spectrometry 226 (2003) 355–368
International Journal of Mass Spectrometry
www.elsevier.com/locate/ijms

# High precision Fe isotope measurements with high mass resolution MC-ICPMS

S. Weyer[a,b,*], J.B. Schwieters[a]

[a] *ThermoFinnigan, Barkhausenstr. 2, D-28197 Bremen, Germany*
[b] *Frankfurt Institut für Mineralogie, Johann Wolfgang Goethe-Universität, Senckenberganlage 28, D-60054 Frankfurt, Germany*

Received 21 October 2002; accepted 31 January 2003

**Abstract**

This study presents a new technique for high precision measurement of iron isotope ratios using high mass resolution MC-ICPMS on the ThermoFinnigan Neptune. A mass resolving power of about 8000–9000 was used to resolve the mass interferences of isobaric polyatomic ions (e.g., $^{40}Ar^{16}O^+$ on $^{56}Fe^+$, $^{40}Ar^{16}OH^+$ on $^{57}Fe^+$ and $^{40}Ar^{14}N^+$ on $^{54}Fe^+$) from the Fe isotopes and to produce "flat top" peak shapes with a plateau width of about 100 ppm in mass ($\Delta m/m$). The abundance sensitivity was determined to 50 ppm contribution of the $^{40}Ar^{16}O^+$ peak tail on the $^{56}Fe^+$ peak. This enables Fe isotope measurements with a Fe-isotope/interference ratio of up to 1, without significant contribution from the tail of the interference peak. The performance of the technique was tested by determining the reproducibility and accuracy of synthetic Fe samples and spiked standards against the IRMM014 standard. Various interface setups, including wet and dry plasma techniques, and a wide range of concentrations (from 50 ppb to 10 ppm) have been used to demonstrate the flexibility, robustness and sensitivity of the technique. An external precision of ca. 0.10‰ for $\delta^{56}Fe$ and ca. 0.15‰ for $\delta^{57}Fe$ (2 S.D.) was routinely achieved. Measured and calculated delta values between spiked standards and the IRMM014 standard agree within uncertainties. In the investigated concentration range, precision and accuracy are independent of both the sample introduction system and the sample concentration. The new technique presented in this study is a robust and simple method to perform high precision Fe isotope measurements, and it allows to measure much lower sample concentrations compared to previous techniques.


*Keywords:* MC-ICPMS; High mass resolution; Iron; Stable isotopes

## 1. Introduction

The interest in stable isotope measurements of transition metals (such as Fe, Cu and Zn) has increased in the last few years in Geo- and Cosmoscience, since improved analytical techniques led to the discovery of natural mass-dependent isotope fractionation [1–17]. Relative mass differences of the various isotopes of the same element are fairly small, resulting in small isotopic fractionations typically in the range of a few per mil. The resolution of these small natural isotope fractionations requires precise and reliable analytical methods. In particular, one has to be careful to distinguish natural isotopic variations from those introduced by the measurement technique itself.

Preferred techniques are thermal ionization mass spectrometry (TIMS) [1,2,12,13] and multiple collector inductively coupled plasma mass spectrometry

* Corresponding author. Tel.: +49-69-798-22548; fax: +49-69-798-28066.
*E-mail addresses:* stefan.weyer@em.uni-frankfurt.de (S. Weyer), Johannes.Schwieters@Thermo.com (J.B. Schwieters).

1387-3806/03/$ – see front matter © 2003 Elsevier Science B.V. All rights reserved.
doi:10.1016/S1387-3806(03)00078-2

(MC-ICPMS) [3,6,8,9,14,16,18–21]. Mass fractionation produced on the filament using TIMS is relatively small in magnitude compared to the mass bias produced by an ICP source (for Fe ca. 3–4% per amu). However, the TIMS mass fractionation is time-dependent and difficult to control. A time consuming double spike technique is necessary to achieve a precision of about 0.2–0.3‰ [1]. The ICP source is characterized by high ionization efficiencies for most elements, including Fe. Mass bias can be kept constant within about 0.1‰ over a short time period, allowing the determination of small differences in isotopic composition between a sample and a standard simply by a sample standard bracketing method [19].

However, particularly for elements in the lower mass range (20–80), including Fe, a major disadvantage of ICP-MS is that most atomic ions suffer from mass interferences of isobaric polyatomic ions (polyatomic interferences), which can limit the precision and accuracy for isotope ratio measurements. Common polyatomic interferences on Fe isotopes are $^{40}Ar^{14}N^+$ on $^{54}Fe^+$, $^{40}Ar^{16}O^+$ on $^{56}Fe^+$, $^{40}Ar^{16}OH^+$ on $^{57}Fe^+$, and $^{40}Ar^{18}O^+$ on $^{58}Fe^+$, respectively. Additional interferences may be introduced by the sample matrix, such as $^{40}Ca^{16}O^+$, $^{40}Ca^{16}OH^+$ or $^{44}Ca^{12}C^+$. Most previous techniques (e.g., [19]) used a desolvating nebulizer technique to suppress oxides and hydroxides. However, a high sample consumption was necessary (within the microgram range) because some interferences could not be completely suppressed.

Here we present a technique of measuring all Fe isotopes simultaneously with high mass resolution, which is the most general approach to completely eliminate interferences by clear spectral separation [20,21]. The ThermoFinnigan Neptune is the first MC-ICPMS instrument which has the capability to achieve high mass resolution in multicollector mode [22]. Various spiked standards and synthetic samples of a large concentration range were measured with “wet” and “dry” plasma conditions. Measurements were performed relative to the IRMM014 Fe standard and delta values were calculated using a simple sample standard bracketing method.

## 2. Instrumental

All measurements were performed using the Neptune ThermoFinnigan MC-ICPMS. The Neptune is a double focusing multiple collector ICP-MS which has the capability of high mass resolution measurements in multiple collector mode [22,23]. A schematic presentation of the Neptune ion optics is shown in Fig. 1. The instrument was equipped with eight motorized Faraday cups and one fixed central channel where the beam can be switched between a Faraday detector and an SEM detector. In situ monitoring of the detector position directly at the optical bench of the multicollector ensures precise and reproducible cup positioning. This is particularly important for high mass resolution measurements. The close coincidence of angular and energy image plane enables the Neptune to perform high mass resolution measurements on all collector positions along the focal plane.

Due to an ion optical magnification of two, a large mass dispersion of 810 mm and an increased focal depth is achieved. The maximum distance between the outermost cup positions corresponds to a relative mass range of 17%. The optical magnification enables the use of larger Faraday cups machined from solid carbon and with a larger effective depth, thereby reducing the emission of secondary ions. The external precision of measurements is further improved by a rotating amplifier concept, in which all Faraday cups are sequentially connected to all amplifiers, canceling out any gain calibration errors. The dynamic range of the amplifiers is extended from 10 to 50 V (using $10^{11}\ \Omega$ resistors) improving the signal to amplifier noise ratio and the precision of high dynamic range isotopic ratio measurements (e.g., $^{58}Fe/^{56}Fe$).

Neptune has three switchable entrance slits located before the ESA (electrostatic analyzer) with slit widths of 250, 30 and 16 μm, resulting in one low and two high mass resolution modes (which are called “medium” and “high” mass resolution). The mass resolution mode can be changed, without switching off the plasma. The plasma interface is held at ground potential (analyzer at −10 kV) allowing easy access to the nebulizer, spray chamber and torch during

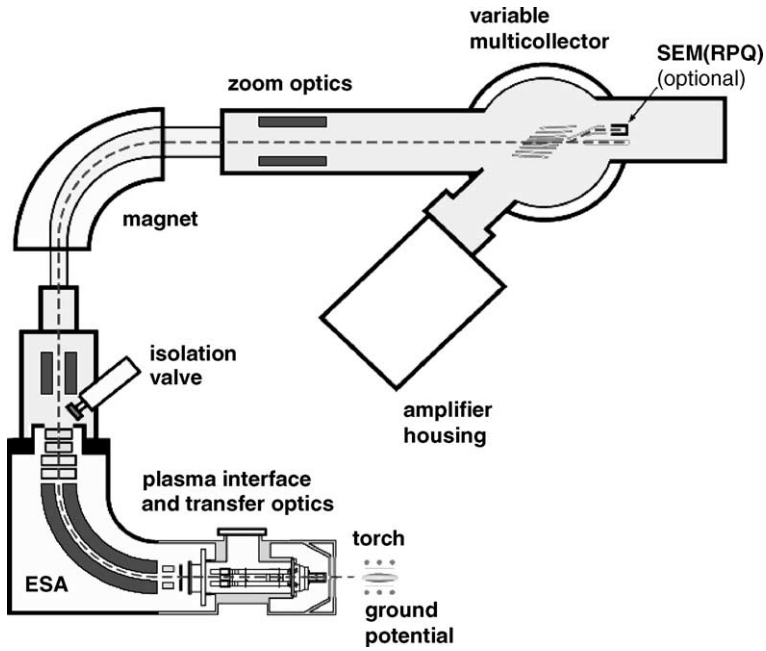


Fig. 1. Schematic presentation of the Neptune ion optics (see text for detailed description).

analyses. The mass bias, which is generated in the plasma interface and the ion transfer optics, is typically about 2% per amu for Li, 3.5% for Fe and 0.6% for U. Mass bias is very constant within the course of a day. A typical daily mass bias variation is <1‰/amu for Fe. Short term (ca. 30 min) mass bias stability, which is more relevant for the sample standard bracketing, is <0.1‰/amu.

Two different types of sample introduction systems were used for the Fe measurements presented in this study, namely the ThermoFinnigan stable introduction system (SIS) and the Cetac Aridus desolvating nebulizer (Table 1). The SIS consists of a tandem quartz glass spray chamber arrangement (cyclone + standard Scott double pass) together with a low-flow (typically 50 μL/min) PFA nebulizer. The SIS gives the most

Table 1
Sample introduction systems used for the Fe measurements

| | Sample introduction | |
|---|---|---|
| | SIS inlet | Aridus |
| Sensitivity with standard (H) cones[a] | 4–6 V | ca. 20–30 V[b] |
| With X-cones | 12–20 V | 50–100 V[b] |
| Washout time (to <1‰) | 2 min | 5–10 min (memory-spikes!) |
| Major interferences | $^{40}Ar^{14}N^+$ on $^{54}Fe^+$, $^{40}Ar^{16}O^+$ on $^{56}Fe^+$, $^{40}Ar^{16}OH^+$ on $^{57}Fe^+$, and $^{40}Ar^{18}O^+$ on $^{58}Fe^+$ | |
| Abundance of interferences[c] | 5–50% | <1% for ArO, ArOH and ca. 100% for ArN[b]<br><1% for $ArO^+$, $ArOH^+$ and $ArN^+$[d] |

[a] For medium mass resolution on $^{56}Fe$ in a 1 ppm Fe-solution using $10^{11}$ Ω resistors.
[b] If N-gas is used to optimize sensitivity and stability.
[c] Relative to the beams of $^{54}Fe$, $^{56}Fe$, $^{57}Fe$ and $^{58}Fe$, respectively, using a 1 ppm Fe solution.
[d] If no N-gas is used (resulting in reduced sensitivity and stability).

stable signal and has fast wash out times (ca. 3 min). The relative intensities of the Ar-based polyatomic ions ($^{40}Ar^{14}N^+$, $^{40}Ar^{16}O^+$, $^{40}Ar^{16}OH^+$, and $^{40}Ar^{18}O^+$) that appear at the same nominal mass as the Fe isotopes ($^{54}Fe^+$, $^{56}Fe^+$, $^{57}Fe^+$, and $^{58}Fe^+$) vary between 5 to 50% of the respective Fe isotope beams for a Fe concentration of 1 ppm (depending on cones and nebulizer used). The Aridus gives a ca. five times higher sensitivity compared to the SIS, however, needs longer washout times. The Aridus suppresses effectively the $ArO^+$ and $ArOH^+$ interferences (to an abundance of <1% for 1 ppm Fe). However, if nitrogen gas is used to optimize the sensitivity the Aridus produces a large $ArN^+$ interference resulting in a $^{54}Fe^+/^{40}Ar^{14}N^+$ ratio of 1–2 for a 1 ppm Fe solution. The Aridus can also be used without nitrogen. However, in this case, the sensitivity is reduced by a factor of 2–10 and the signal stability is poorer as well.

Typical ion beams on $^{56}Fe^+$ in medium mass resolution and using standard (H) cones for a 1 ppm Fe solution are ca. 4–6 V (using the SIS) and 20–30 V (using the Aridus) (Table 1). In low mass resolution, the sensitivity is about a factor of 6–7 higher and in high mass resolution, a factor of 2 lower compared to the medium mass resolution mode. 400–500 ng of Fe are needed for an analysis of ca. 5 min in medium mass resolution, when the SIS together with standard cones are used. With a recent development in cone geometry (X-cones), the sensitivity was further improved by a factor of ca. 3. Combining the X-cones with the Aridus inlet system, a sensitivity of ca. 50–100 V (3–6 GHz) on $^{56}Fe^+$ (1 ppm Fe) can be achieved in medium mass resolution, which is of particular interest for low concentration samples. With a typical uptake rate of 50 μL/min, this corresponds to a transmission for Fe in medium mass resolution of ca. 0.5‰.

## 3. Elimination of polyatomic mass interferences

### 3.1. Previous strategies

Previous strategies of interference reduction are, e.g. (1) desolvating nebulizer, (2) collision cells (or chemical reaction cells) or (3) measuring with “cold plasma” conditions. All methods suppress spectral interferences only partially:

(1) Desolvating nebulizers are commonly used for Fe isotope measurement. They produce a dry plasma with low oxide and hydroxide formation (e.g., ArO, ArOH). However, the only commercially available desolvating nebulizer, the Cetac Aridus, needs nitrogen gas to optimize sensitivity and signal stability. In this case, large nitrogen-based interferences are produced (e.g., NO, ArN), of which $ArN^+$ interferes with $^{54}Fe^+$. Therefore, if analyzing Fe, the Cetac Aridus has to be used under non-optimal conditions without nitrogen gas. Even then the Aridus does not completely suppress ArO, ArOH and ArN. Therefore, high sample loads (e.g., 5–40 ppm [19]) are necessary to achieve a high and constant signal to background ratio.

(2) Collision cells have also successfully been used for Fe [3,16]. They have the potential to break some Ar-based molecular interferences and to suppress the Ar ions. However, new interferences and blanks can potentially be generated in the collision cell itself. Also the collision cell acts as an additional source of mass bias.

(3) At low plasma power (e.g., 600 W, also known as “cold plasma”) the Ar-based ion species are significantly reduced, since Ar has a very high first ionization potential. Since most elements have a much lower first ionization potential, cold plasma is a suitable method to reduce the relative abundance of Ar-based interferences. Cold plasma produces also a significantly lower mass bias (e.g., for Fe, the mass bias is about a factor of 2 lower compared to hot plasma conditions). However, we found the cold plasma mass bias to be less stable and more sensitive to changes in sample concentration and sample matrix. Up to 5‰ difference in the measured $^{56}Fe/^{54}Fe$ was observed between a 1 and a 10 ppm solution of the same Fe standard measured in cold plasma. Although the $Ar^+$ species and $ArO^+$ are drastically

reduced, some interferences, such as $ArN^+$ or $ArOH^+$ are not completely suppressed. Potential interferences from the sample matrix, including $CaO^+$ or $CaN^+$ are not suppressed at all. Therefore, cold plasma may be useful for very specific applications but the matrix-dependent mass bias effects can be a pitfall, if precise isotope ratio measurements are desired.

### 3.2. High mass resolution multicollector measurements

The classical way of high mass resolution measurements on single collector sector instruments is to use a narrow entrance slit and a narrow detector (or exit) slit. The latter is just wide enough (or even smaller) to catch the complete ion beam profile in the focal plane of the mass spectrometer. This results in triangular peakshapes without any flat plateaus. The most accepted definition for mass resolution is the 10%-valley definition: According to this definition, two adjacent peaks of the same intensity and with a mass difference $\Delta m$ are resolved, as long as they do not overlap in a mass spectrum by more than 10% of the peak intensities (measured in the valley, which is formed between the peaks). The 10%-valley definition is therefore a measure for the peak separation power of a mass spectrometer and is suitable for scan mode measurements.

High precision isotope ratio measurements using an ICP source require complete interference suppression, but also simultaneous measurements of the isotopes on "flat top" peak shapes in a static multicollection mode. Flat top peak shapes are an indispensable prerequisite for high precision isotope ratio measurements. On triangular peak shapes, tiny drifts of the magnet and the HV, which cannot be completely eliminated, result in reduced signal stability and poor precision.

To achieve flat top peak shapes it is necessary (1) to use an entrance slit, which is sufficiently small to get an interfering free space between the ion beams in the focal plane and (2) to use detector slits that are wider than the ion beam profiles in the focal plane of the mass spectrometer. Wider detector slits result in a poorer mass resolution (according to the 10%-valley definition), with wider peak widths in a mass scan. However, the wider the detector slits, the larger are the flat plateaus of the peaks in a mass scan. If the detector slits are wider than the distance between two resolved ion beams in the focal plane, the peaks appear unresolved in a mass scan. However, the flat plateaus achieve their maximum width, which is independent of the width of the collector slit.

In practice, this setup can be achieved with a high mass resolution entrance slit (to resolve the ion beams in the focal plane) and low mass resolution detector slits (e.g., with $m/\Delta m = 400$ according to the 10%-valley definition). Such an arrangement is

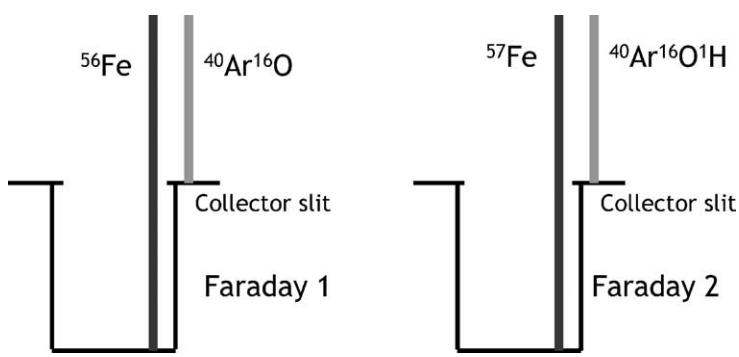


Fig. 2. Schematic presentation of the collector setup used for the simultaneous measurement of $^{56}Fe$ and $^{57}Fe$ using a high resolution entrance and low resolution collector slits. The high resolution entrance slit clearly resolves the Fe isotopes from their respective polyatomic interferences. The resolved Fe isotopes are simultaneously collected at the edge position of the Faraday cups, while the polyatomic interferences do not enter the detectors.

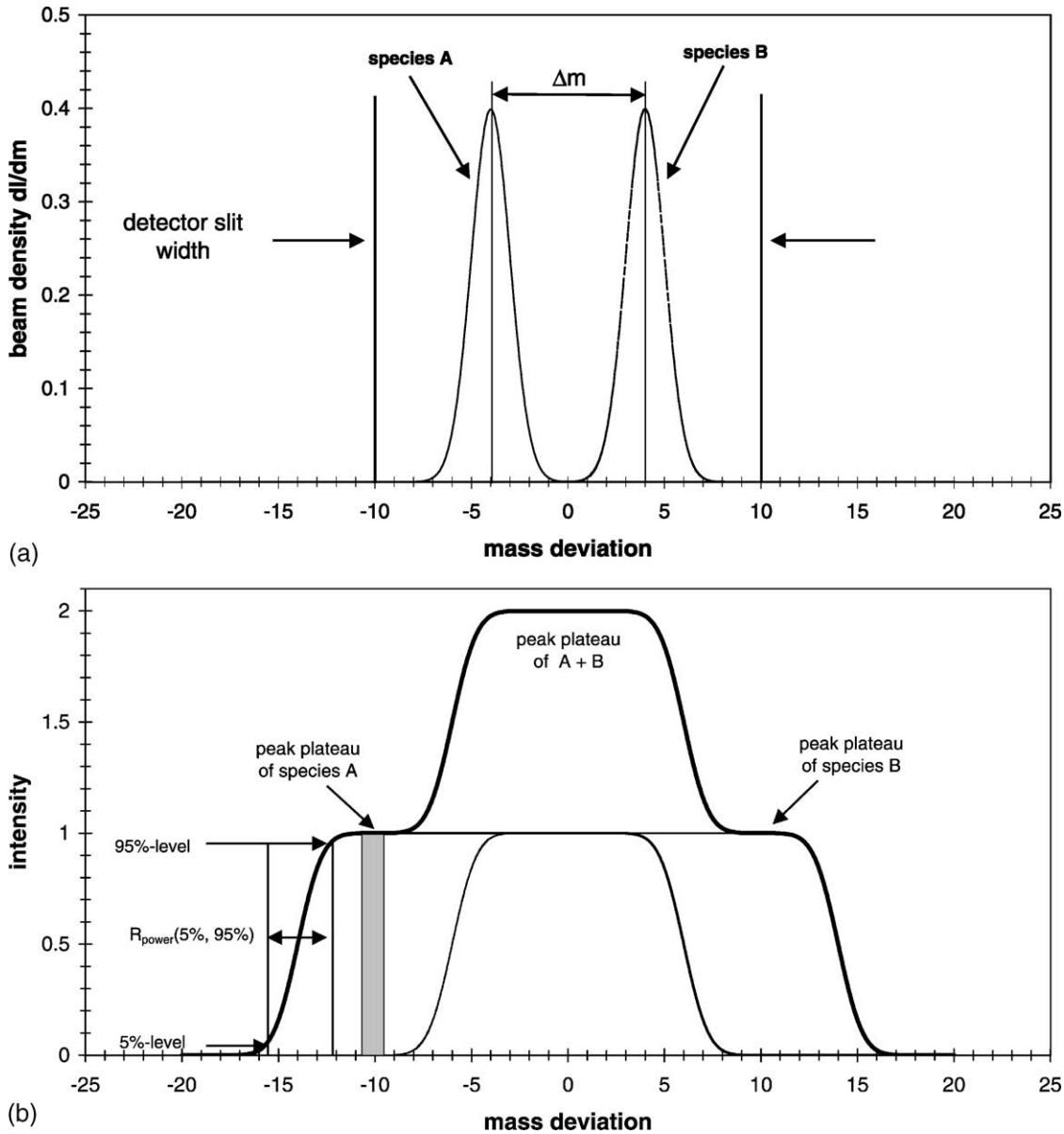


Fig. 3. (a) Ion beam profiles at the detector side of the mass spectrometer of two ion species A and B with a mass difference of $\Delta m$. The beams are separated by the use of a high resolution entrance slit (narrow slit width). The detector slit (indicated by the two solid vertical lines) is set at low mass resolution mode (wide slit width). (b) Recorded peak profile, when the adjacent ion beam profiles of ion species A and B with a mass difference of $\Delta m$ are scanned across the low resolution detector slit. First the lighter ion species A enters the detector slit and forms the first plateau section of the peak, which is indicated by the gray shadowed rectangle. At that time the heavier ion species B is still clipped at the high mass side of the detector slit. The second plateau section appears when both ion beams enter the detector slit. This is the situation of (a). Finally, the ion beam A is clipped on the low mass side of the detector slit and only species B enters the cup and forms the third plateau section. The resolving power $R_{\text{power}}(5, 95\%)$ is given by the distance of the two vertical lines.

schematically shown in Fig. 2. In a mass scan, the interfering species appear as discrete steps with flat top peak sections. This is illustrated in Fig. 3b (schematic mass scan), where two ion species A and B with a mass difference of $\Delta m$ are considered. Fig. 3a is the first derivative of Fig. 3b and represents the ion beam profiles of the two ion species, A and B. The ion beam profiles in the focal plane can be approximated by a Gaussian density distribution.

In order to come to a definition of mass resolution which is independent of the selected detector slit width (the mass resolution according to the 10%-valley definition depends on both: the entrance and detector slit width), we propose to measure the width of the ion beam profile in the focal plane where the detector slits are positioned (Fig. 3b). This mass resolution definition is an expression of the resolving power of the mass spectrometer.

We define the resolving power to be:

$$R_{\text{power}}(5,\ 95\%) = \frac{m}{\Delta m^*} = \frac{m}{m(5\%) - m(95\%)}$$

with $m(5\%)$ is the mass at 5% of peak height, $m(95\%)$ is the mass at 95% of peak height, $m$ is the mass of the peak.

The higher the resolving power, the smaller the ion beam profile at the detector slit (Fig. 3a) and the steeper the peak slope (Fig 3b). The higher the resolving power relative to the mass resolution required to separate two ion species, the broader will be the flat plateau region, which represents the interference-free space between the ion beams. A high resolving power is mainly achieved by closing down the entrance slit, at the expense of transmission. Therefore, the entrance slit width has to be small enough to achieve a flat plateau, but at the same time large enough to achieve sufficiently high transmission. It can be estimated from Fig. 3a and b, that the resolving power $m/\Delta m^*$ has to be at least a factor of 2 higher than the $m/\Delta m$ of the species A and B, to ensure a flat plateau section of A and B.

In the case of static multicollection with a variable multicollector mass spectrometer, each detector can be positioned individually to discriminate the interfering ion species at the edge of the detector slit so that the undisturbed beam hits the detector in the center of the plateau section (Fig. 4). This method of high mass resolution measurement works as long as all interfering species appear only on one side of the

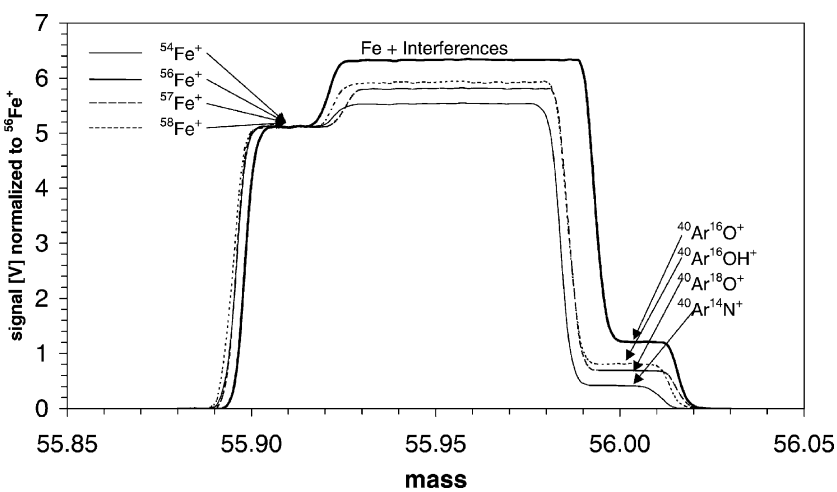


Fig. 4. Mass scan performed with the Neptune's "medium resolution" entrance slit and "low resolution" collector slits" showing all Fe isotopes and their respective molecular interferences. All Fe signals are normalized to the signal of $^{56}$Fe. Since the Fe isotopes have a lower mass, they enter the detector first in a scan and form the left plateau. The center plateau consists of polyatomic interferences added to the Fe isotopes. The right plateau is formed by the polyatomic interferences only. Fe isotope ratios can be measured interference-free on left plateau. The scan was performed on a 1 ppm Fe solution, using the SIS (wet plasma) and standard (H) cones.

undisturbed ion beam. If interferences appear on both sides of the ion species of interest, this method would not work. Fortunately, nature is kind and all polyatomic interferences up to a mass of ca. 90 amu are heavier than the respective elemental species (including Mg, Si, Ca, Cr, Fe, Cu and Zn). This is also true for 2+ ions of all elemental species with a mass of >45 amu (for elements < mass 45, e.g., Mg and Si, the 2+ ions are on the lower mass side).

### 3.3. High mass resolution Fe isotope ratio measurements

To resolve all Fe isotopes from the common polyatomic interferences, such as $^{40}Ar^{14}N^+$, $^{40}Ar^{16}O^+$, $^{40}Ar^{16}OH^+$ and $^{40}Ar^{18}O^+$ a mass resolution of about 2500 would be sufficient. Noteworthy, all possible interferences (including 2+ ions) are heavier than the respective Fe isotopes and therefore appear on the same side of the Fe peaks.

With the technique described in Section 3.2, flat resolved peak sections are defined and the Fe isotopes can be measured at the edge position of the Faraday cups, where the polyatomic interferences are completely eliminated. Fig. 4 shows a peak scan of all Fe isotopes and their polyatomic interferences, which was performed using the Neptunes "medium" mass resolution entrance and the low mass resolution collector slit. As demonstrated by the peak scan all Fe isotopes are affected by polyatomic interferences. The most important ones are indicated in the diagram. A resolving power of about 8000–9000 can be achieved with the "medium" mass resolution slit (Fig. 5). This results in sufficiently wide plateaus for Fe isotope measurements, since the resolving power is about a factor of 3–4 higher than the $m/\Delta m$ of the Fe isotopes and their respective interferences. Using the "high" mass resolution slit would increase the resolving power to about 10,000–12,000, however, reducing the sensitivity by a factor of 2 at the same time.

The width and flatness of the Fe plateaus has been tested by measuring Fe isotope ratios at different positions on the plateaus. Fig. 5, a blow up of Fig. 4, shows a mass scan over the Fe plateaus, with all Fe

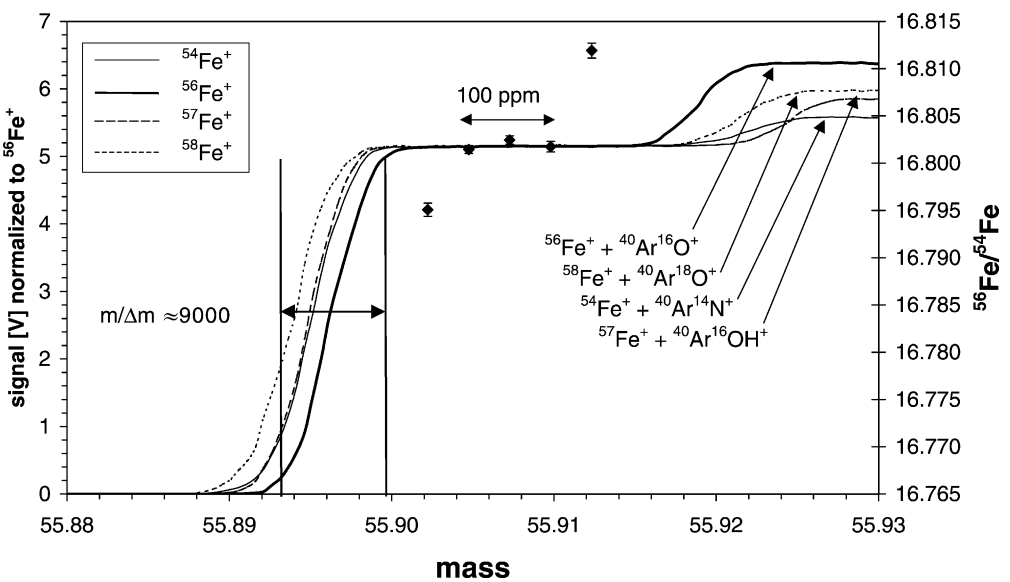


Fig. 5. Plateau flatness test: the mass scan over the Fe-plateau with signals normalized to $^{56}Fe$ (left scale) is a blow up of the peakscan shown in Fig. 4. The resolving power in medium resolution was about 9000. Also included into the plot are $^{56}Fe/^{54}Fe$ ratios (diamonds) measured at various positions on the Fe plateau (right scale). The three measurements performed at the center part of the plateau agree within their uncertainties, indicating a real "flat plateau" of ca. 100 ppm ($\Delta m/m$).

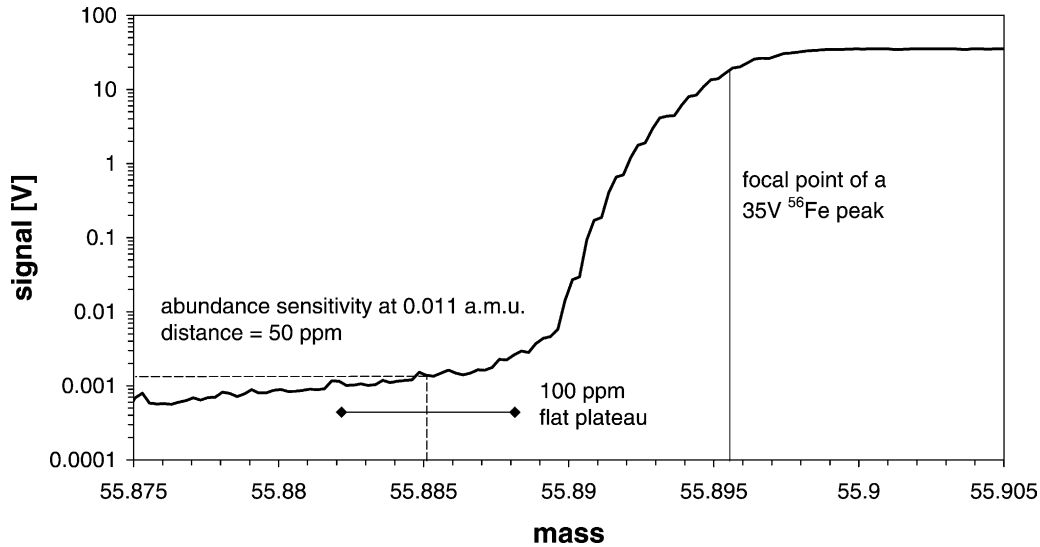


Fig. 6. Abundance sensitivity in medium mass resolution measured at the low mass side of the $^{56}Fe$ peak. The abundance sensitivity is measured at a distance of 0.011 amu from the focal point of the $^{56}Fe$ peak, which corresponds to the distance from the $^{40}Ar^{16}O$ focal point to the center of the $^{56}Fe$ plateau, where the Fe isotope ratios are measured. It corresponds to exactly half of the distance between the separated $^{56}Fe$ and $^{40}Ar^{16}O$ ion beams at the detector plain. The position of the 100 ppm flat plateau (here relative to the $^{56}Fe$ and not to the $^{40}Ar^{16}O$ peak), which was determined in Fig. 5 is also indicated in the plot.

signals normalized to the signal of $^{56}Fe^+$ (left *Y*-axis). Shown within the same plot are $^{56}Fe/^{54}Fe$ ratios (right *Y*-axis) measured at the various positions. Both ratios obtained from either edge of the plateaus differ significantly (ca. 0.4–0.6‰) from the value achieved at the center of the plateaus. However, the ratios of three measurements performed around the center position of the plateau agree within their uncertainties (ca. 30 ppm 1 S.D.), defining a flat plateau of about 100 ppm in mass ($\Delta m/m$).

The abundance sensitivity for high mass resolution Fe measurements can be expressed as the contribution of the $^{40}Ar^{16}O^+$ tail on the center of the $^{56}Fe^+$ plateau, where $^{56}Fe$ is measured. The abundance sensitivity was determined at the low mass side of $^{56}Fe^+$ at a distance, equal to the distance from the focal point of the $^{40}Ar^{16}O^+$ peak to the center of the $^{56}Fe^+$ plateau (ca. 11 millimasses). This distance corresponds exactly to half of the distance between the focal points of the $^{56}Fe^+$ and the $^{40}Ar^{16}O^+$ peak. In Fig. 6, the abundance sensitivity at that mass difference can be determined to be about 50 ppm. This means that for a $^{56}Fe^+/^{40}Ar^{16}O^+$ ratio of 5 (as in Figs. 4 and 5), the contribution from the $^{40}Ar^{16}O^+$ tail on the middle of

Table 2
Collector configuration used for the Fe high mass resolution measurements

| | Nominal mass | | | | | |
|---|---|---|---|---|---|---|
| | 52 | 54 | 56 | 57 | 58 | 60 |
| Measured elements | | Fe | Fe | Fe | Fe | |
| Natural abundance (%) | | 5.8 | 91.75 | 2.2 | 0.28 | |
| Interfering elements | Cr | Cr | | | Ni | Ni |
| Natural abundance in (%) | 83.789 | 2.365 | | | 68.27 | 26.10 |
| Cup-configuration | L4 Faraday | L2 Faraday | Center faraday | H1 Faraday | H2 Faraday | H4 Faraday |

the $^{56}Fe^+$ plateau, where the Fe is measured, is about 10 ppm.

The collector configuration used to measure all Fe isotopes simultaneously is shown in Table 2. $^{53}Cr^+$ and $^{60}Ni^+$ are also measured simultaneously to monitor and correct the isobaric interferences of $^{54}Cr^+$ on $^{54}Fe^+$ and $^{58}Ni^+$ on $^{58}Fe^+$. These elemental interferences cannot be resolved with high mass resolution, because mass resolution of ca. 68,000 and 28,000 ($m/\Delta m$), respectively, would be required.

## 4. Results and discussion

For the evaluation of the performance of the method, the Fe isotope composition of various samples were measured and delta values were calculated referring to the Fe standard IRMM014. The results are shown in Tables 3 and 4, and Fig. 7. The external precision was calculated from replicate measurements of the standard materials relative to IRMM014. The three synthetic Fe solutions (Table 4) were provided to us by F. von Blanckenburg (University of Hannover, Germany): JM was prepared from a Fe wire supplied by Johnson Matthey; AKA-4 (akaganeite) was produced by slow precipitation of FeOOH from a Merck Fe(III)$Cl_3 \times 6H_2O$-solution; FeOOH-7 (ferryhydrite) was oxidized in air at 70 °C from a Fluka Fe(II)$Cl_2 \times 4H_2O$-solution [24]. To check the accuracy of the delta values, two differently spiked Fe standards were produced by adding a small amount of an isotopic tracer (IRMM620), which is enriched in $^{57}Fe$, to the Fe standard IRMM014 (Table 3, Fig. 7). The isotopic composition of the spiked standards (spikes 1 and 2) were calculated from the isotope compositions of the pure spike (IRMM620) and the standard (IRMM014).

Most of the measurements were performed with Neptune's "medium" mass resolution setting, which

Table 3
Precision and accuracy of two spiked standards relative to IRMM014, measured with various concentrations and various sample introduction systems (delta values in ‰)

| Method | Spike-1 | | Spike-2 | | |
|---|---|---|---|---|---|
| | $\delta^{56}Fe/^{54}Fe$ | $\delta^{57}Fe/^{54}Fe$ | $\delta^{56}Fe/^{54}Fe$ | $\delta^{57}Fe/^{54}Fe$ | $\delta^{58}Fe/^{54}Fe$[a] |
| SIS | | | | | |
| 10 ppm Fe-concentration[b] | 0.01 | 0.85 | 0.02 | 8.26 | 1.45 |
| 2 S.D. | 0.04 | 0.05 | 0.02 | 0.07 | 0.16 |
| 3 ppm Fe-concentration | 0.02 | 0.88 | | | |
| 2 S.D. | 0.04 | 0.04 | | | |
| Aridus | | | | | |
| 1 ppm Fe-concentration | 0.01 | 0.80 | −0.03 | 8.31 | |
| 2 S.D. | 0.02 | 0.08 | 0.08 | 0.17 | |
| Aridus with X-cones | | | | | |
| 200 ppb Fe-concentration | 0.01 | 0.83 | −0.05 | 8.28 | |
| 2 S.D. | 0.03 | 0.03 | 0.09 | 0.13 | |
| 50 ppb Fe-concentration[c] | 0.02 | 0.84 | | | |
| 2 S.D. | 0.04 | 0.10 | | | |
| Mean of all measurements | 0.01 | 0.84 | −0.02 | 8.28 | 1.45 |
| 2 S.D. (of all measurements) | 0.03 | 0.08 | 0.09 | 0.12 | 0.16 |
| Calculated | 0.00 | 0.82 | 0.00 | 8.20 | 1.40 |

2 S.D. is calculated from 3 to 5 replicate measurements.

[a] The $^{58}Fe/^{54}Fe$ was only evaluated for the 10 ppm spike-2 were $^{58}Fe$ intensity was >50 mV. The $^{58}Fe/^{54}Fe$ of spike-1 was not resolvable from IRMM014 within analytical uncertainties.

[b] The 10 ppm Fe-concentration data were performed with "high" all others with "medium" mass resolution.

[c] The 50 ppb spike-1 was measured relative to 200 ppb IRMM014, whereas all other spike measurements were performed relative to concentration-matched IRMM014 standard solutions.

Table 4
Delta values (in ‰) of three synthetic Fe samples relative to IRMM014, measured with various concentrations and various sample introduction systems

| Method | JM-metal | | AKA-4 | | FeOOH-7 | |
|---|---|---|---|---|---|---|
| | $\delta^{56}Fe/^{54}Fe$ | $\delta^{57}Fe/^{54}Fe$ | $\delta^{56}Fe/^{54}Fe$ | $\delta^{57}Fe/^{54}Fe$ | $\delta^{56}Fe/^{54}Fe$ | $\delta^{57}Fe/^{54}Fe$ |
| SIS | | | | | | |
| 3 ppm Fe-concentration | 0.28 | 0.46 | −0.63 | −0.95 | 3.12 | 4.61 |
| 2 S.D.[a] | 0.07 | 0.13 | 0.11 | 0.17 | 0.06 | 0.15 |
| Aridus | | | | | | |
| 1 ppm Fe-concentration | 0.41 | 0.60 | −0.59 | −0.87 | 3.17 | 4.67 |
| 2 S.D.[a] | 0.06 | 0.01 | 0.01 | 0.07 | 0.08 | 0.08 |
| Aridus with X-cones | | | | | | |
| 200 ppb Fe-concentration | 0.40 | 0.60 | −0.62 | −0.92 | 3.11 | 4.59 |
| 2 S.D.[a] | 0.08 | 0.09 | 0.02 | 0.05 | 0.07 | 0.17 |
| Mean of all measurements | 0.35 | 0.54 | −0.61 | −0.92 | 3.13 | 4.62 |
| 2 S.D. (of all measurements) | 0.14 | 0.16 | 0.08 | 0.13 | 0.09 | 0.14 |
| Reference[b] | 0.46 | 0.68 | −0.58 | −0.91 | 3.23 | 4.83 |

[a] 2 S.D. is calculated from 3 to 5 replicate measurements.
[b] Reference values are from F. von Blankenburg (personal communication and [24]) measured with the Nu Plasma MC-ICPMS (University of Bern, Switzerland).

was sufficient to resolve the molecular interferences (as described above). For comparison, only the measurements of the 10 ppm spike-1 and spike-2 solution were performed with Neptune's "high" mass resolution setting. All delta values were measured using the sample/standard bracketing method (standard–sample–standard–sample . . . ). It was also tested to use Cu and Ni for mass bias correction

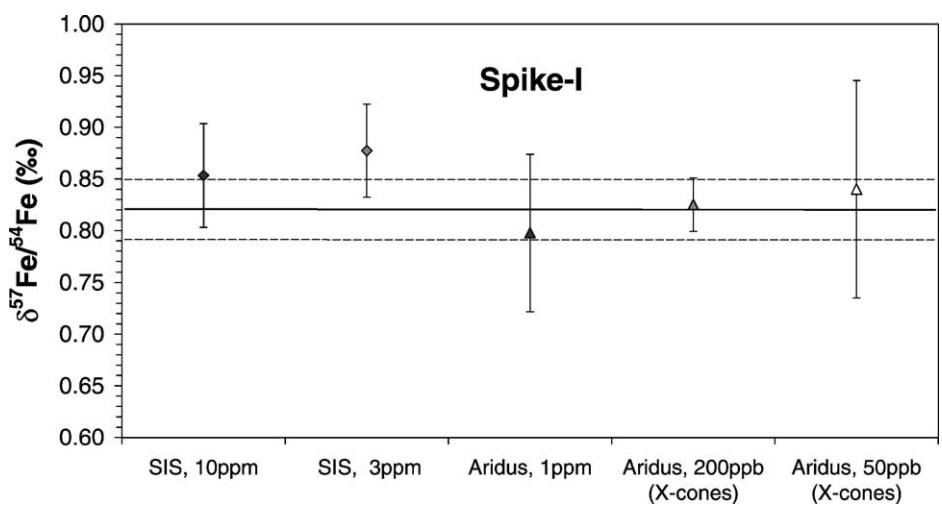


Fig. 7. Comparison of spike-1 $\delta^{57}Fe$ values (relative to IRMM014) measured with wet (SIS) and dry plasma (Cetac-Aridus) at different sample concentrations: (1) SIS, 10 ppm, H-cones; (2) SIS, 3 ppm, H-cones; (3) Aridus, 1 ppm, H-cones; (4) Aridus, 200 ppb, X-cones; (5) Aridus, 50 ppb, X-cones; (1) was measured with the "high" mass resolution, all others with the "medium" mass resolution entrance slit. For (1)–(4) samples and standard concentrations were matched; however (5) (the 50 ppb sample) was measured against a 200 ppb standard. Each data point consists of 3–5 measurements; error bars represent 2 S.D. external reproducibilities. The solid line represents the calculated value for spike-1 and the dotted lines the uncertainty on the calculated value.

(using the exponential law or the method described in Maréchal et al. [4]). However, this did not significantly improve the external precision of the delta values for the pure Fe solutions, which were used for this study. Mass bias correction using Cu can be useful, if samples with a complex matrix are measured, even if most of the matrix has been chemically separated before (Anbar et al., in preparation).

The variation of the measured $^{56}Fe/^{54}Fe$ and $^{57}Fe/^{54}Fe$ of one standard within a day and between several days can be clearly attributed to variations in mass bias and not to variable interference contribution (with the exception of the lowest sample concentration measurements using the Aridus with nitrogen gas, where a background correction was performed). This is demonstrated by Fig. 8, where $\ln(^{56}Fe/^{54}Fe)$ was plotted vs. $\ln(^{57}Fe/^{54}Fe)$. The IRMM014 standard measurements, performed over three consecutive days, fit excellently to a linear regression line with a slope close to 1.5 (as theoretically expected from the ratio of the relative mass differences of $(^{56}Fe–^{54}Fe)/^{54}Fe$ and $(^{57}Fe–^{54}Fe)/^{54}Fe$). All measurements in Fig. 8 were performed, using a ThermoFinnigan SIS and standard cones to introduce a 3 ppm Fe solution into the plasma. The mass bias was usually stable over several hours. Occasionally, a constant drift in the range of 0.2‰/h was observed. With the sample–standard bracketing method, mass bias drift was completely canceled out and no difference in precision was observed, between days with either drifting or constant mass bias.

Typical reproducibilities for replicate measurements of delta values was $<0.10$‰ (2 S.D.) for $\delta^{56}Fe$ and $<0.15$‰ (2 S.D.) for $\delta^{57}Fe$ (Tables 3 and 4). Both spiked standard solutions agreed within their uncertainties with the calculated values, which is evidence for both, the high precision and accuracy achieved with the presented technique. The results are independent of the sample concentration and no systematic difference was observed between the values obtained with the SIS (wet plasma) and the Aridus interface (dry plasma). This emphasis the superior robustness of the high mass resolution method compared to previous methods. Despite the loss of sensitivity, related to the higher mass resolution (due to the use of a smaller entrance slit), sensitivity was sufficiently high to precisely measure the Fe isotope composition on sample concentrations as low as 50 ppb. For these low sample concentrations, the Aridus combined with X-cones have been used.

For most delta measurements sample and standard concentrations were matched within ±10%

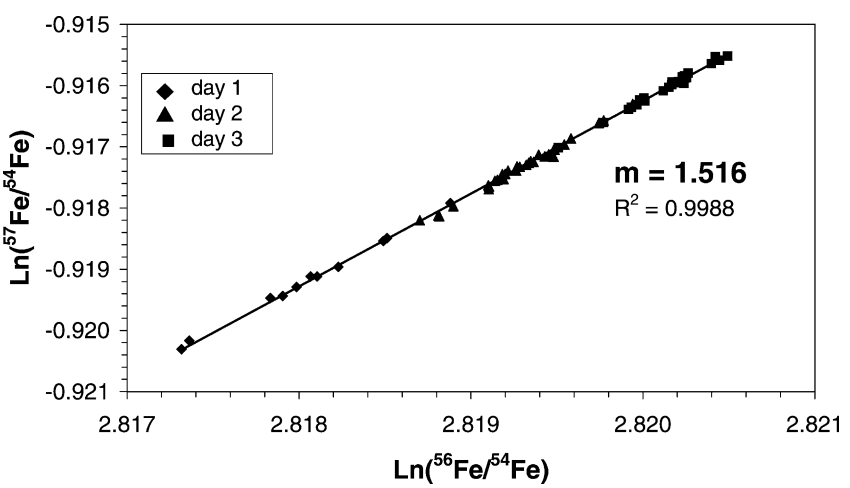


Fig. 8. Plot of $\ln(^{56}Fe/^{54}Fe)$ vs. $\ln(^{57}Fe/^{54}Fe)$ of 3 ppm IRMM014 standard measurements, performed over there consecutive days with the SIS spray chamber and standard cones. All measurements have a close fit to a linear regression line with a slope of ≈1.5, demonstrating that variations are only mass bias, but not interference related.

(with the exception of the 50 ppb spike-1 sample) and therefore, background subtraction was not necessary (a background subtraction is already included in the delta value calculation for matched sample and standard concentration). This works with sufficient precision, since the background contribution (using high/medium mass resolution) is usually negligible. For most measurements, the background was only determined for monitoring (by measuring a blank solution) at the beginning and end of a sequence or every few hours.

The background measured for Fe consists of three components: (1) The electronic noise, which is most relevant for $^{58}$Fe. Since the noise does not vary during a standard sample standard cycle to more than ca. 5 μV, the uncertainty introduced to a >100 mV beam is <50 ppm. (2) The Fe instrument memory (from nebulizer, spray chamber, injector, torch and cones), which was always <2 mV (on $^{56}Fe^+$) and therefore <1‰, after a washout of ca. 3 min, if using the SIS. A higher instrument memory was occasionally observed if the Aridus was used. Since the variation in the isotopic composition of the Fe samples is <1%, the contribution of the instrument memory to the uncertainty is <10 ppm, if using the SIS. (3) The tail of the interfering beam, which becomes relevant (>50 ppm), if the intensity of the interference is bigger than the intensity of the Fe beam.

Typical background measurements for SIS and Aridus (with the nitrogen gas to optimize the $Fe^+$ signal) are shown in Table 5. Using the SIS, the isotope ratios of the background are similar to the Fe isotope ratios. This indicates, that most of the background is Fe and that polyatomic interferences are almost completely suppressed. It can be calculated from the abundance sensitivity (Fig. 5), that the contribution of polyatomic interferences to a 1 ppm Fe solution is only 5–20 ppm, when using the SIS. Using the Aridus with nitrogen gas, background ratios are significantly different from Fe. The difference is produced by the tail of the ArN interference. For low Fe concentrations, the $ArN^+$ interference can be much bigger than the $^{54}Fe^+$ signal, resulting in a significant tail contribution. In this case, a separate background correction is advisable.

With a background correction high precision Fe isotope measurements can be achieved, even for (1) very low Fe concentrations and (2) if the concentration between sample and standard are not matched. This is demonstrated with the measurement of a 50 ppb Fe (spike-1) solution relative to a 200 ppb (IRMM014) standard (Table 3, Fig. 7). The $ArN^+$ beam was about 20 times that of the beam on $^{54}Fe^+$ (ca. $3 \times 10^{-12}$ A, using X-cones). Therefore, the $ArN^+$ tail contribution on $^{54}Fe^+$ was about 1‰. For this experiment, blank measurements were bracketed with the standard and the sample measurements (blank–standard–blank–sample–blank . . . ).

The results of the synthetic Fe samples agree within uncertainties with the reference values given by F. von Blanckenburg (personal communication and [24]). The reference values were measured with a Nu Plasma MC-ICPMS in low mass resolution and using a Cetac Aridus [17]. However, compared to the low mass resolution technique combined with the Aridus [6,17,19], much lower iron concentrations can be measured with the high mass resolution techniques, presented in this study. Furthermore, no sample–standard concentration matching is required and measurements can be performed with either wet or dry plasma.

Table 5
Typical blanks measured with the SIS and the Aridus after 3 min washout

| | $^{53}$Cr (mV) | $^{54}$Fe(+$^{54}$Cr) (mV) | $^{56}$Fe (mV) | $^{57}$Fe (mV) | $^{58}$Ni(+$^{58}$Fe) (mV) | $^{60}$Ni (mV) | $^{56}$Fe/$^{54}$Fe (mV) | $^{57}$Fe/$^{54}$Fe (mV) |
|---|---|---|---|---|---|---|---|---|
| SIS (wet) | 0.016 | 0.086 | 1.320 | 0.039 | 0.238 | 0.079 | 16.12 | 0.476 |
| Aridus (dry)[a] | 0.028 | 0.791 | 8.780 | 0.194 | 0.281 | 0.137 | 11.20 | 0.247 |

[a] The Aridus was used with nitrogen gas.

## 5. Conclusions

High mass resolution MC-ICPMS has been demonstrated to be a robust method for high precision iron isotope measurements, using the ThermoFinnigan Neptune. Polyatomic interferences on the iron peaks are completely resolved by high mass resolution (using the Neptunes "medium" or "high" mass resolution mode). Wide flat top peak sections are achieved by closing down the entrance slit, but leaving the detector slits at low mass resolution mode. This technique allows a high flexibility of the interface setup to optimize sensitivity. No desolvating nebulizers or other interference suppression techniques are necessary. The presented technique is particularly suited for low concentration samples. A sample consumption of ca. 20 ng of Fe is sufficient to perform high precision isotope ratio measurements with an external reproducibility of $<0.1‰$ (2 S.D.) on $\delta^{56}$Fe.

## Acknowledgements

We are particularly grateful to F. von Blanckenburg (University of Hannover) for providing three synthetically fractionated Fe samples. We thank an anonymous reviewer for constructive comments. F. von Blanckenburg and A. Anbar are thanked for comments on earlier versions of the manuscript.

## References

[1] B.L. Beard, C.M. Johnson, Geochemica et Cosmochemica Acta 63 (1999) 1653.
[2] L.B. Beard, C.M. Johnson, L. Cox, H. Sun, K.H. Nealson, C. Aguilar, Science 285 (1999) 1889.
[3] B.L. Beard, C.M. Johnson, J.L. Skulan, K.H. Nealson, L. Cox, H. Sun, Chem. Geol. (2002), special issue, in press.
[4] C.N. Maréchal, P. Telouk, F. Albarede, Chem. Geol. 156 (1999) 251.
[5] C.N. Maréchal, E. Nicoslas, C. Douchet, F. Albarède, G-cubed 1 (2000).
[6] A.D. Anbar, J.E. Roe, J. Barling, K.H. Nealson, Science 288 (2000) 126.
[7] A.D. Anbar, K.A. Knap, J. Barling, Anal. Chem. 73 (2001) 1425.
[8] X.-K. Zhu, R.K. O'Nions, Y. Guo, B.C. Reynolds, Science 287 (2000) 2000.
[9] X.-K. Zhu, Y. Guo, R.K. O'Nions, E.D. Young, H.D. Ash, Nature 412 (2001) 311.
[10] X.K. Zhu, Y. Guo, R.J.P. Williams, R.K. O'Nions, A. Matthewsa, N.S. Belshaw, G.W. Canters, E.C. de Waal, U. Weser, B.K. Burgess, B. Salvato, Earth Planet. Sci. Lett. 200 (2002) 47.
[11] G.L. Barling, A.D. Arnold, A.D. Anbar, Earth Planet. Sci. Lett. 193 (2001) 447.
[12] S.L. Brantley, L. Liermann, T.D. Bullen, Geology 29 (2001) 535.
[13] T.D. Bullen, A.F. White, C.W. Childs, D.V. Vivit, M.S. Schulz, Geology 29 (2001) 699.
[14] M. Sharma, M. Polizzotto, A.D. Anbar, Earth Planet. Sci. Lett. 194 (2001) 39.
[15] C. Siebert, T.F. Nägler, J.D. Kamers, G-cubed 2 (2001).
[16] C.M. Johnson, B.L. Beard, N.J. Beukes, C. Klein, J.M. O'Leary, Contrib. Mineral. Petrol. 144 (2003) 523.
[17] T. Walczyk, F. von Blankenburg, Nature 295 (2002) 2065.
[18] C.M. Johnson, J.L. Skulan, B.L. Beard, H. Sun, K.H. Nealson, P.S. Braterman, Earth Planet. Sci. Lett. 195 (2002a) 141.
[19] N.S. Belshaw, X.K. Zhu, Y. Guo, R.K. O'Nions, Int. J. Mass Spectrom. 197 (2000) 191.
[20] S. Weyer, J.B. Schwieters, G. Jung, R. Pesch, M. Hamester, Goldschmidt Meeting, J. Conf. Abstr. (2001).
[21] S. Weyer, J.B. Schwieters, Goldschmidt Meeting, J. Conf. Abstr. (2002) A831.
[22] J.B. Schwieters, M. Hamester, G. Jung, R. Pesch, L. Rottmann, S. Weyer, EUG, J. Conf. Abstr. (2001).
[23] J.B. Schwieters, M. Hamester, G. Jung, R. Pesch, L. Rottmann, D. Tuttas, J. Wills, Neptune: a new high precision multicollector ICP mass spectrometer, Goldschmidt Meeting, J. Conf. Abstr. 5 (2000) 899.
[24] F. von Blanckenburg, M.E. Böttcher, Eur. J. Mineral. (Beihefte) 13 (2001) 193.